The evaporation of sessile droplets onto solid surfaces : experiments and simulations of the contact line pinning-depinning

L.Kabeya-Mukeba, N.Vandewalle and S.Dorbolo
GRASP, Institut de Physique B5a, University of Liège, B-4000 Liège, Belgium.
(Dated: May 21, 2007)

Sessile water droplets onto various surfaces are observed during their evaporation at room temperature. The pinning of the contact line is emphasized in (V, θ) and (R, θ) diagrams in which droplet evaporation is a curve. The late stages of evaporation seem to be characterized by an asymptotic droplet radius R_{min} while the contact angle decreases far below the Young contact angle $\theta^\star$. Our experimental results are then confronted to a model able to reproduce 'evaporation trajectories' in (R, θ) diagrams. The major ingredients of the model are quasi-static equilibrium and the presence of an attractive potential. We show that the strength of this potential could be measured in experiments through a parameter λ, thus providing a practical way to characterize solid interfaces and to understand the depinning.

PACS numbers: 61.30.Hn, 68.03.Fg, 68.08.Bc

I. INTRODUCTION

The evaporation of water droplets is a natural phenomenon which plays an important role in various systems like water cycles and plant transpiration. Evaporation is a complex phenomenon involving various physical processes like surface effects, heat transfer [1, 2], diffusion [3], contact line instabilities [4], convection [5], etc... Evaporation is also a crucial parameter when one considers modern applications like new open microfluidic devices, self-cleaning materials and fire protection in combustion science [6].

Most evaporation studies [1-15] deal with pure liquids on hydrophobic and hydrophilic surfaces.Only a few works consider liquid mixtures [2]. Authors mainly focuss their efforts to follow the evolution of both contact angle θ and droplet radius R as a function of time t [1, 9–12]. Most works concern volatile liquids exhibiting a fast evaporation [4]. Droplets containing colloidal suspensions are also of interest since evaporation leaves various patterns onto the solid surface [13–15].

The motion of the contact line during droplet evaporation is the subject of numerous studies [16]. The contact line motion can exhibit various regimes : advancing, pinning and receding [11]. Those regimes depends on various physical parameters such as surface energies, heat transfer, and surface roughness [17, 18]. Figure 1(left) presents 6 pictures of an evaporating droplet of pure water onto a horizontal glass plate. Two successive pictures are separated by one minute. The first four pictures illustate the pinning of the contact line while the contact angle decreases. The last two pictures show the receding motion of the contact line with a small contact angle. For this sequence of pictures, the depinning occurs at the right side of the droplet. A similar droplet on a mylar sheet exhibits a similar pinning-depinning behavior (see Figure 1(right)).

In this paper, we focuss our attention on both pinning and receding regimes like those illustrated in Figure 1. We are interested by water evaporation since water is the main solvant in natural and applied sciences. The aim of our study is to emphasize and to characterize experimentally the pinning-depinning of the contact line. A spherical cap model will be studied. This allows us to discuss the mechanisms of water droplet evaporation.

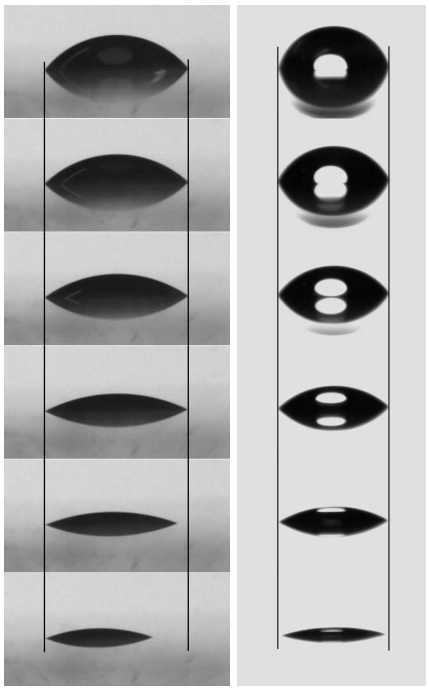

FIG. 1: (left) Sequence of 6 images of a water droplet onto a glass plate during evaporation. Two successive images are separated by 60 seconds. In the first 4 images, the contact angle is observed to decrease while the contact line is pinned. In the last two pictures, the droplet is seen to recede with a nearly constant contact angle. (right) Sequence of 6 images of a water droplet onto a mylar sheet during evaporation. Two successive images are separated by 180 seconds. Vertical lines emphasize the pinning of the droplet. The distance between both vertical lines is 2 mm.

II. EXPERIMENTAL RESULTS

A. Experimental set-up

We are interested in the possible shape variations of the droplet during evaporation. Particularly, the pinning of the contact line will be studied. The study of the evaporation kinetics is not concerned by this work. The kinetics depends on numerous parameters like the room temperature T and relative humidity of air RH [3]. Those parameters are herein fixed to $T = 25°\mathrm{C}$ and $RH = 45\%$ in atmospheric pressure conditions.

In order to follow the evaporation of droplets, we used a contact angle meter (CAM200 from KSV Ltd) based on image analysis. After calibration, this equipment is able to calculate the main geometrical characteristics of the droplet like the volume, the radius and the contact angle. All measurements have been made at room temperature. Droplets of various volumes are placed onto various horizontal surfaces : glass plates and mylar sheets. Droplets are generated by a syringe. Pendant droplets are then gently placed onto the surface before removing the needle. The free evaporation of droplets is video recorded and the images are then treated numerically. Typically, the time separating two successive analyzed images is 30 seconds. The contact line keeps its circular shape during evaporation. Non-axisymetric droplets [19] are outside the scope of this work.

B. Glass plates

The first surfaces, we have investigated, are glass plates. Before placing a droplet onto a glass plate, the surface is cleaned with acetone and with pure water before drying. In order to keep the system as clean as possible, droplets are never placed at the same place onto the surface. Figure 2(top) exhibits the evolution of the contact angle θ as a function of the droplet volume V. Different initial volumes V_0 are illustrated on the figure. Initial contact angles are in the range $50° < \theta < 60°$. In all cases, the contact angle is seen to decrease when the evaporation takes place. When the droplet becomes smaller than a critical volume or when the contact angle becomes smaller than a critical value, the slope of the evaporation curve changes drastically. This change has to be attributed to the depinning of the contact line. This is revealed in the next figure. Figure 2(bottom) shows the evolution of the contact angle θ as a function of the droplet radius R. The droplet radius is a constant at the beginning of the evaporation process. This motionless behavior is the pinning of the contact line. For small contact angles, the depinning occurs at $\theta \approx \theta_c$ and the radius decreases rapidly while the contact angle seems to be nearly a constant. The critical contact angles seem to depends on the volume of the considered droplet and are in the range $20° < \theta_c < 30°$.

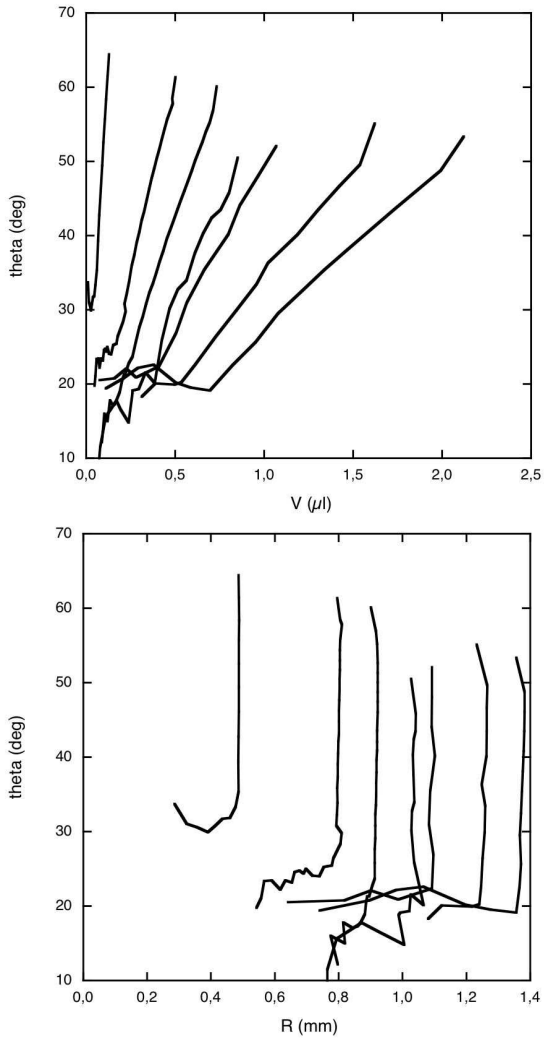

FIG. 2: Evaporation of seven water droplets on glass plates. (top) The contact angle of various water droplets as a function of their volume V. Each curve represents an evaporation. (bottom) The contact angle of various water droplets as a function of the radius R of the contact circle. The vertical part of each curve represents pinning during evaporation.

C. Mylar sheets

The second kind of surfaces that we have investigated are mylar sheets. Figure 3(top) exhibits the evolution of the contact angle as a function of the droplet volume. When the droplet is gently placed onto the surface, the contact angle is roughly $\theta \approx 80°$ whatever the droplet volume. The contact angle is seen to decrease when the evaporation goes on. Figure 3(bottom) shows the evolution of the contact angle as a function of the droplet radius R.

The curves are similar to previous ones obtained onto glass substrates. The depinning occurs at larger angle values ($50° < \theta_c < 60°$). This allows us to better capture the receding motion of the droplet. In that case, the

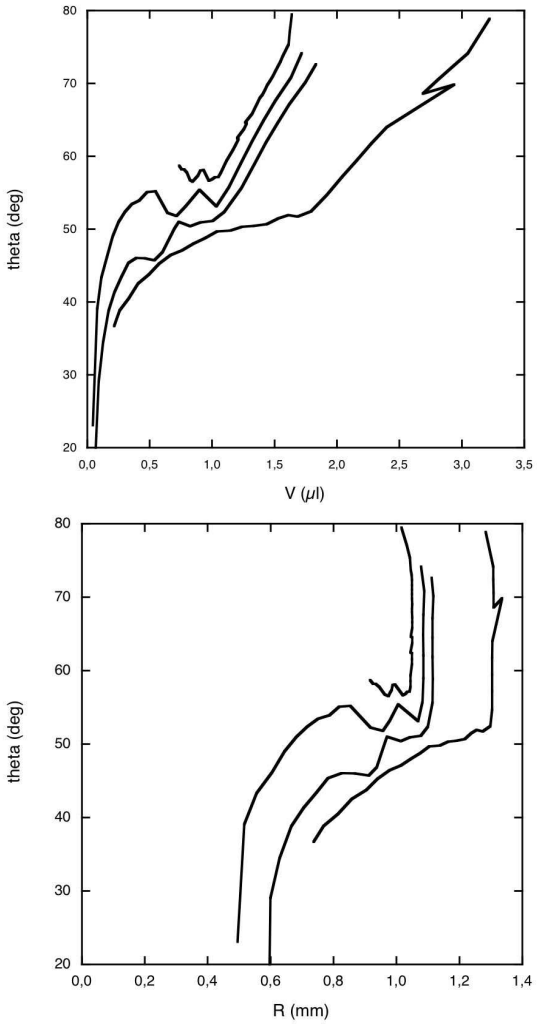

FIG. 3: Evaporation of four water droplets on mylar sheets. (top) The contact angle of various water droplets as a function of their volume V. Each curve represents an evaporation. (bottom) The contact angle of various water droplets as a function of the radius R of the contact circle. The vertical part of each curve represents pinning during evaporation.

contact angle is seen to still decrease when the contact line is depinned. The receding dynamics shows always a decrease of θ with a negative curvature. Moreover, one can observe a vertical behavior during the late stages of some $\theta(R)$ curves. This suggests the existence of a minimum radius $R_{min} \approx 0.5$ mm for small θ values. This will be discussed at the end of this paper. We do not obtain reproducible measurements for $\theta < 10°$. Another dewetting process may occur for such very small contact angle.

D. Other surfaces

Similar pinning-depinning features have been observed on various surfaces like polyvinyl chloride and nylon surfaces. Figure 4 presents a single evaporation curve in the (R, θ) diagram for a polyvinyl chloride surface. The sampling rate for the measurements has been reduced to 15 seconds in order to increase precision. Nevertheless, large fluctuations of θ are still observed after the depinning. Those large zigzag structures could be attributed to some stick-slip of the contact line [20].

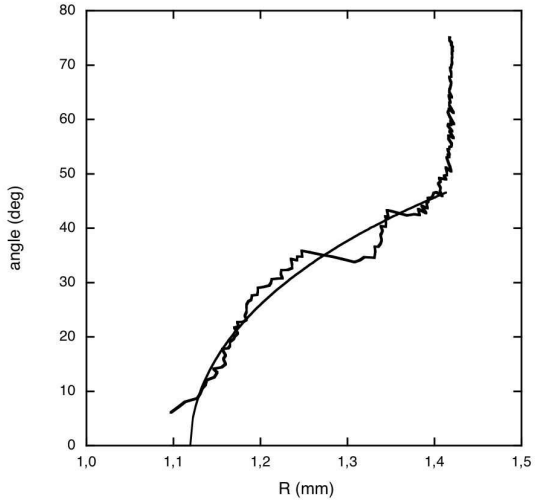

FIG. 4: Evaporation of a water droplet on a polyvinyl chloride surface. Large fluctuations are observed during the receding dynamics. However, the overal receding behavior can be fitted with the Eq.(12) with parameters $\theta^\star = 120°$ and $\lambda = 12.3\,10^{-5}$ J/m.

It should be noted that evaporation experiments have been also performed on teflon surfaces. On that particular hydrophobic surfaces, no pinning was observed. The $\theta(R)$ curves are quite different and will not be examined herein.

III. NUMERICAL RESULTS

A. Spherical cap model

In summary, we have characterized the pinning of the contact line of evaporating droplets in (θ, R) diagrams. Such diagrams exhibit typical evaporation curves with measurable features. In order to capture the physical ingredients behind droplet evaporation, we have developed a numerical model which is original and is easy to implement. The model is based on two simple assumptions described below.

Firstly, the evaporation is assumed to be slow enough to consider a quasi-static equilibrium at each stage of the process. For each evaporation stage, one should consider the energy minimization of the system. This assumption is valid for water droplets at room temperature, for which the evaporation rate is slow : dV/dt being typically a few nanoliters per second.

Secondly, the droplet shape is assumed to be a spher-

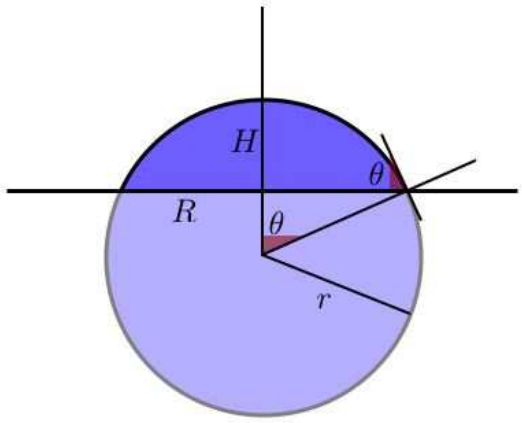

FIG. 5: The model considers a droplet as a spherical cap of volume V and characterized by a contact angle θ. Different length scales are considered : H, H_c and R.

ical cap, as described by Figure 5. The center of the sphere has a variable vertical position. The spherical cap shape should be valid for tiny droplets less sensitive to gravity. This assumption will be discussed below since we decided to include the effect of gravity in the model. The droplet of volume V is thus characterized by its radius r and the contact angle θ. One has

$$V = \frac{\pi r^3}{3}\left[2 - 3\cos\theta + \cos^3\theta\right]. \quad (1)$$

This spherical cap could be also characterized by the vertical position of its top point

$$H = r\left[1 - \cos\theta\right], \quad (2)$$

the height of the centroid, i.e. the center of gravity

$$H_c = \frac{3r}{4}\frac{(1+\cos\theta)^2}{(2+\cos\theta)}, \quad (3)$$

and the radius of the circular contact line

$$R = r\sin\theta. \quad (4)$$

Those three characteristic lengths (H, H_c and R) are functions of both r and θ.

The energy of the system is thus given by

$$U = \gamma_{lg}A + (\gamma_{sl} - \gamma_{sg})A' + \rho g V H_c \quad (5)$$

where the various terms represents different sources of potential energy. All terms of Eq.(5) depends on both variables θ and r. The first term represents the surface energy of the spherical cap (area A). The parameter γ_{lg} is the surface tension of the liquid phase, i.e. $\gamma_{lg} = 0.073\,\mathrm{J/m^2}$ for pure water. The area of the dome is given by

$$A = 2\pi r^2\left[1 - \cos\theta\right], \quad (6)$$

The second term of Eq.(5) represents the adhesion energy along the contact area A'. This area is given by

$$A' = \pi r^2 \sin^2\theta. \quad (7)$$

The last term of Eq.(5) represents the effect of gravity ($g = 9.81\,\mathrm{m/s}$). The density ρ of the liquid is then an important parameter fixed herein to $\rho = 1000\,\mathrm{kg/m^3}$ (water density).

Our algorithm starts with a fixed volume $V = V_0$. By expressing all areas with θ and R, instead of θ and r, we can minimize the energy as a function of θ with a constant volume. The contact angle minimizing the energy is recorded and the new droplet shape is calculated. Then, the volume of the droplet is reduced by a small quantity ($V \to V - \delta V$). Those stages are repeated until the droplet is completely evaporated.

Our numerical approach is straightforward and does not consume lots of power computing like vertex algorithms [21, 22]. It has also the advantage to be easily implemented to various situations such as non-uniform surfaces and inclines. This is left for future works.

B. Gravity effect

Starting with any volume V_0 and for a set of physical parameters ($\gamma_{lg}, \gamma_{sl} - \gamma_{sg}$), the droplet shape tends rapidly to a spherical cap characterized by an equilibrium contact angle $\theta^\star$ given by the Young's relation

$$\cos\theta^\star = -\frac{\gamma_{sl} - \gamma_{sg}}{\gamma_{lg}}. \quad (8)$$

This behavior is shown in Figure 6 where $\theta/\theta^\star$ is plotted as a function of the droplet radius R. The small difference between θ and $\theta^\star$ should be attributed to the effect of gravity which tends to "crush" the droplet onto the surface. As a consequence, one has always $\theta < \theta^\star$. Of course, this effect is more pronounced for large droplets (when R becomes larger than the capillary length). It should be also noted that this effect is more pronounced for large contact angles.

For tiny droplets close to the ones observed in our experiments, the effect of gravity concerns only a few percentages of $\theta^\star$. The effect of gravity is therefore marginal for our study.

C. Pinning of the contact line

Since the expression (5) cannot describe the main features like the contact line pinning during droplet evaporation, we decided to consider an additional term to the energy. This term is a pinning potential. The total energy reads

$$U = \gamma_{lg}A + (\gamma_{sl} - \gamma_{sg})A' + \rho g V H_c + 2\pi\lambda|R - R'| \quad (9)$$

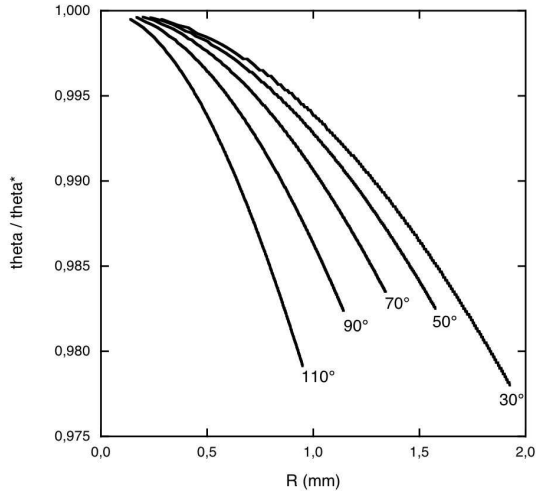

FIG. 6: The ratio of the contact angle θ and the equilibrium contact angle $\theta^\star$ during evaporation for different initial situations : $V_0 = 3\,\mu$l and $\theta^\star = 30°, 50°, 70°, 90°, 110°$.

where λ is some energy by unit length and R' being the last position of the contact line. The factor $2\pi|R - R'|$ is the variation of length of the contact line. In order to move the contact line (or change its length), it costs some energy λ per unit length. This pinning energy is the same for advancing and receding contact lines. It should be noted that theoretical studies [23, 24] of contact line deformations lead to similar anchoring energies. The reality is of course more complex and an asymetric potential can be considered.

Some (V, θ) curves are shown in Figure 7(top). The curves are similar to what we observed in section 2. The (R, θ) curves are presented in Figure 7(bottom). They are quite similar to our observations (compare with Figures 2 and 3). All curves exhibit pinning followed by a receding motion. Since various types of potential energy compete in Eq.(9), one understands that pinning occurs when $\lambda > \gamma_{lg} R$. Taking the pinning energy $\lambda \approx \gamma_{lg} R$ into account, realistic evaporation curves can be generated by our model.

On Figure 7(bottom), one can observe a master curve for the receding dynamics. This master curve seems to be independant of V_0. This evaporation trajectory will be analyzed in the next section.

It should be noted that inflating the droplet is also possible within this model. This leads to a depinning with an advancing contact angle higher than $\theta^\star$. It is therefore possible to reproduce contact angle hysteresis by the model, taking into account the new parameter λ.

IV. DISCUSSION

Our experiments have emphasized the pinning of the contact line. The pinning-depinning phenomenon is well described by our model and is captured by only one parameter λ being some energy by unit length.

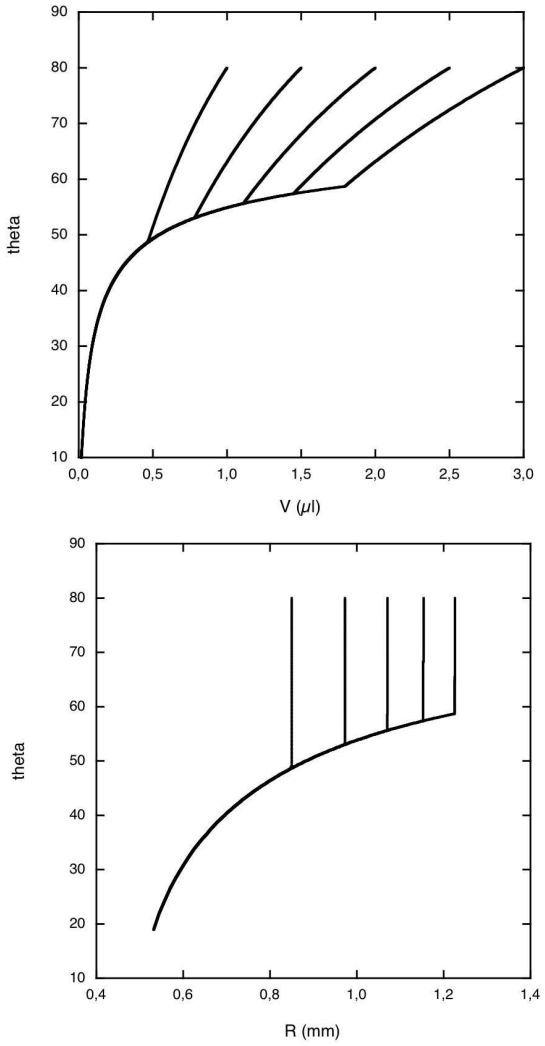

FIG. 7: Numerical simulations of water droplet evaporation for various initial volumes $V_0 = 1.0\,\mu\text{l}, 1.5\,\mu\text{l}, 2.0\,\mu\text{l}, 2.5\,\mu\text{l}, 3.0\,\mu\text{l}$. The pinning energy parameter lambda is fixed to $\lambda = 2\,10^{-5}$ J/m. (top) Droplet volume - contact angle diagram. (bottom) Droplet radius - contact angle diagram.

The results could be interpreted by taking the derivatives of the potential energy. In the following, the effect of gravity is neglected. When only dome and surface energies compete, both R and θ variables are decorrelated. Indeed, the equilibrium condition reads

$$dU = 0 \;=\; 2\pi(\gamma_{sl} - \gamma_{sg}) R\, dR + \frac{2\pi\gamma_{lg}}{1+\cos\theta} R\, dR + \;2\pi\gamma_{lg} R^2 \frac{\sin\theta}{(1+\cos\theta)^2}\, d\theta \qquad (10)$$

By considering a constant volume for the spherical cap ($dV = 0$), one has the additional condition

$$\frac{d\theta}{dR} = -\frac{\sin\theta(2+\cos\theta)}{R} \qquad (11)$$

TABLE I: Typical values of the pinning energy parameter λ.

solid surface	$\theta^\star$	λ (J/m)
glass	$\approx 60^\circ$	$3\,10^{-5}$
mylar sheet	$\approx 80^\circ$	$4\,10^{-5}$
polyvinyl chloride	$\approx 120^\circ$	$12\,10^{-5}$

which is obtained by taking the first derivative of Eq.(1). Both conditions lead to the Young equilibrium relationship (8). Therefore, a droplet has a contact angle $\theta^\star$ whatever its radius R when the last term of Eq.(9) is absent.

Taking the anchoring potential into account (see Eq.(9)) leads similarily to the equilibrium condition for the contact angle

$$\theta = \arccos\left(\frac{\lambda}{R\gamma_{lg}} + \cos\theta^\star\right) \tag{12}$$

when dR is non-zero, i.e. after depinning. Otherwise, the pinning $dR = 0$ is allowed by both $dU = 0$ and $dV = 0$ conditions. This behavior predicts also a fixed minimum value R_{min} of the droplet radius for the late stage of evaporation. One has

$$R_{min} = \frac{\lambda}{\gamma_{lg}(1 - \cos\theta^\star)} \tag{13}$$

This behavior could be observed experimentally in some cases. It can be seen in Figure 3 (bottom) for $\theta > 10^\circ$. In experiments (see Figure 3(bottom)), slight differences appear between different evaporation curves, meaning that the solid surface is heterogeneous. However, the curves (see Figure 4) are well fitted by Eq.(12). The table 1 gives typical values of λ obtained on different substrate. Eventhough λ is a macroscopic parameter, which does not take microscopic surface roughness into account, this parameter gives a good idea of the energy barrier encountered by the contact line.

V. CONCLUSION

In summary, we have performed reproducible experiments of evaporating water droplets. The depinning of the contact line is observed in (θ, R) diagrams. A model is proposed for reproducing experimental evaporation curves. A new parameter λ characterizes the pinning energy. This parameter could be estimated by fitting the data with numerical simulations.

The numerical model is quite simple in its actual form. It could be generalized in order to simulate contact angle hysteresis and more complex phenomena associated with droplets onto solid surfaces. A more detailed model considering non-spherical droplets is under development by our team.

Acknowledgments

SD would like to thank FNRS for a financial support. This work has been also supported by the contract ARC 02/07-293.

[1] K.Hisatake, S.Tanaka, and Y.Azaway, J. Appl. Phys. **73**, 7395 (1993)
[2] K.Sefiane, L.Tadrist and M.Douglas, Int. J. Heat and Mass Transfer **46**, 4527 (2003)
[3] H.Hu and R.G.Larson, J. Phys. Chem. **106**, 1334 (2002)
[4] C.Poulard, O.Bénichou and A.M.Cazabat, Langmuir **19**, 8828 (2003)
[5] J.J.Hegseth, Phys. Rev. E **54**, 1640 (1996)
[6] H.Zhang, Combustion Sc. Technol. **175**, 2237 (2003)
[7] L.M.Hocking, Phys. Fluids **7**, 2950 (1995)
[8] S.J.S.Morris, J. Fluid Mech. **432**, 1 (2001)
[9] K.S.Birdi, D.T.Vu, and A.Winter, J. Phys. Chem. **93**, 3702 (1989)
[10] K.S.Birdi and D.T.Vu, J. Adhesion Sci. Technol. **7**, 485 (1993)
[11] C.Bourgès-Meunier and M.E.R.Shanahan, Langmuir **11**, 2820 (1995)
[12] H.Y.Erbil, G.McHale, and M.I.Newton, Langmuir **18**, 2636 (2002)
[13] R.D.Deegan, O.Bakajin, T.F.Dupont, G.Huber, S.R.Nagel, and T.A.Witten, Nature **389**, 827 (1997)
[14] R.D.Deegan, O.Bakajin, T.F.Dupont, G.Huber, S.R.Nagel, and T.A.Witten, Phys. Rev. E **62**, 756 (2000)
[15] R.D.Deegan, Phys. Rev. E **61**, 475 (2000)
[16] P.G.deGennes, Rev. Mod. Phys. **57**, 827 (1985)
[17] J.Bico, C.Tordeux and D.Quéré, Europhys. Lett. **55**, 214 (2001)
[18] T.Cubaud and M.Fermigier, Europhys. Lett. **55**, 239 (2001)
[19] G.McHale, N.J.Shirtcliffe and M.I.Newton, Langmuir **20**, 10146 (2004)
[20] M.E.Shanahan, Langmuir **11**, 1041 (1995)
[21] K.Brakke, http://www.susqu.edu/facstaff/b/brakke/evolver/
[22] N.A.Patankar and Y.Chen, in Proceedings of the 5th International Conference on Modeling and Simulation of Microsystems, (San Juan, Puerto Rico, 2002)
[23] J.F.Joanny and P.G.deGennes, J.Chem. Phys. **81**, 552 (1984)
[24] P.G.deGennes, F.Brochart-Wyart, D.Quéré, *Gouttes, bulles, perles et ondes*, (Belin, Paris, 2002)